Acta Materialia 265 (2024) 119624

Contents lists available at ScienceDirect

Acta Materialia

journal homepage: www.elsevier.com/locate/actamat

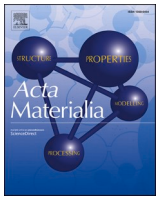

Full length article

Structural building-blocks of disordered Cu-Zr alloys

W. Porter Weeks [a], Katharine M. Flores [a,b,*]

[a] Institute of Materials Science and Engineering, Washington University in St. Louis, MO, United States
[b] Department of Mechanical Engineering and Materials Science, Washington University in St. Louis, MO, United States

ARTICLE INFO

Keywords:
Metallic glass
Molecular dynamics simulations
Amorphous materials
Glass forming ability

ABSTRACT

The atomic structures of Cu-Zr alloys have been extensively studied due to the unusually high glass forming ability of this system. In this work, we investigate the nearest-neighbor atomic structures of several simulated disordered Cu-Zr compositions at three temperatures: 1450 K (liquid), 700 K (undercooled liquid), and 350 K (disordered solid). The results show that over 90 % of the local structures in these systems can be described by one of 12 "building-block" atomic cluster geometries, regardless of composition or temperature, and that these structures all exhibit icosahedral or quasi-icosahedral geometries. Most of the building-blocks are unique in their combination of representative Voronoi polyhedron geometry, predominant central atom type, and occupation probability for each site in the cluster. In addition to the 12 common building-blocks, 35 "outlier" structures unique to their simulated compositions and temperatures were observed. The outliers were primarily non-icosahedral. While the populations of the common building-blocks do not exhibit clear trends with temperature or composition, the overall population of outliers increased with decreasing temperature, suggestive of their role in accommodating the lack of translational order in the disordered solid.

1. Introduction

Bulk metallic glasses (BMGs) exhibit an interesting combination of properties such as high elastic strain limits, near-theoretical strengths, and thermoplastic formability that make them desirable for numerous applications [1,2]. One of the challenges with formulating structure-property models for BMGs is reliably describing their structure. Early work on disordered liquids by Bernal [3,4] focused on the geometric arrangement of randomly packed spheres. Using a physical model analogous to placing hard spheres of equal size into a flexible bag and squeezing it until there is no discernable change in volume, Bernal investigated "contacts" and "close-contacts" of local atomic environments, which yielded less than 10 structure types describing all of the observed packing geometries [3]. Later work showed strong agreement between simulated radial distribution functions of these structures and x-ray diffraction patterns of experimental metallic glasses [5,6]. Gaskell's stereochemical model considered the medium-range connectivity of trigonal "building-blocks" within transition metal-based metallic glasses and related this connectivity to glass-forming ability (GFA) of metallic alloys [7]. In both cases, a surprisingly small number of fundamental building-blocks within metallic liquids and/or metallic glasses were identified [8]. Recently, Weeks and Flores built on this preliminary work, showing that the nearest-neighbor atomic structures within macroscopically disordered metallic liquids can be described by a small number of representative cluster geometries [9]. One of the alloy systems of interest in that work was Cu-Zr, which has been extensively studied due to the presence of multiple BMG compositions (e.g., $Cu_{50}Zr_{50}$, $Cu_{64}Zr_{36}$) [10–14]. The general interest in Cu-Zr motivates deeper consideration of the building-blocks in this system beyond the prior analysis of simulated Cu-Zr glasses [15,16].

Prior research has suggested that icosahedral geometries are of particular interest in glassy alloys. Sheng and Ma identified "icosahedral-like" structures in simulated metallic glasses [17] which were then confirmed experimentally [18–22]. While the gradual evolution of structure during cooling is expected in amorphous alloys, Wessel et al. showed evidence of unexpected *rapid* chemical ordering in $Cu_{46}Zr_{54}$ undercooled liquids, specifically reporting an increase in Cu-centered icosahedral structures near 850 °C upon cooling [23], although Dai et al. later reported contradictory results and called into question the validity of such a rapid onset in icosahedral order [24]. Further, Cheng et al. used simulations to show the gradual evolution of icosahedral ⟨0,0,12,0⟩ Voronoi clusters upon cooling in $Cu_{46}Zr_{54}$ and $Cu_{46}Zr_{47}Al_7$ liquids, hypothesizing that the reason for higher GFA in the later system is related to the stabilization of icosahedral geometries [25]. All of these

* Corresponding author.
E-mail address: floresk@wustl.edu (K.M. Flores).

https://doi.org/10.1016/j.actamat.2023.119624
Received 17 July 2023; Received in revised form 18 December 2023; Accepted 19 December 2023
Available online 19 December 2023

studies show clear evidence of structural evolution in icosahedral geometries upon cooling in Cu-Zr alloys. In addition to pure icosahedra (⟨0,0,12,0⟩), a series of studies have focused on quasi-icosahedral Voronoi polyhedra in various metallic systems, leading to the identification of various icosahedral-like structures (i.e. ⟨0,1,10,2⟩, ⟨0,1,10,4⟩, ⟨1,0,9,3⟩, ⟨0,2,8,1⟩, ⟨0,2,8,2⟩, and ⟨0,3,6,3⟩) [26–30] exhibiting coordination numbers (CN) between 11 and 15. Focusing on the $Cu_{50}Zr_{50}$ glass-forming alloy, Li et al. investigated the evolution of simulated structures upon cooling and discovered many of these quasi-icosahedral geometries among the local structures, where Cu-centered structures generally exhibited lower CN than Zr-centered structures. Furthermore, Li et al. reported both the persistence of these geometries upon cooling from the liquid state and the evolution of medium-range connectivity upon cooling [31].

While the prior work on icosahedral and quasi-icosahedral geometries in Cu-Zr alloys and the evolution of these structures upon cooling has improved our understanding of GFA, it is based on the use of Voronoi tessellation to describe the topology of the entire structure. As reported previously, Voronoi indices are less useful as descriptors of nearest-neighbor atomic cluster geometry – *i.e.,* the structural building-blocks – particularly in the case of the simulated metallic liquid [9]. A more reliable methodology can be found in a combination of Point Pattern Matching (PPM) and Hierarchal Density-Based Spatial Clustering of Applications with Noise (HDBSCAN) algorithms [15,16]. Furthermore, previous research has focused on specific Cu-Zr glass-formers such as $Cu_{46}Zr_{54}$ [23–25] and $Cu_{50}Zr_{50}$ [31] rather than analyzing a variety of alloy compositions across the binary. In this work, we use the PPM/HDBSCAN method to extract representative nearest-neighbor atomic clusters from the comparison of several simulated Cu-Zr compositions at three temperatures, with the ultimate goal of describing the geometries of these building-blocks and investigating their evolution upon cooling. We show that icosahedral-like geometries describe most short-range structures in Cu-Zr alloys, regardless of composition and temperature, and find that such geometries are not isolated to previously reported glass-formers. The result is 12 fundamental structure types that are fully representative of 90.2 % of all short-range structures in any disordered Cu-Zr alloy, liquid or glassy.

2. Methods

2.1. Molecular dynamics simulations

MD simulations were performed on various Cu-Zr compositions using the Large-scale Atomic/Molecular Massively Parallel Simulator (LAMMPS) [32] and a widely applicable Finnis-Sinclair (FS) interatomic potential was utilized [33]. Thirteen compositions in the range of $Cu_{10}Zr_{90}$ – $Cu_{90}Zr_{10}$ were simulated at increments of 10 at. % for Zr-rich ($Cu_{10}Zr_{90}$ - $Cu_{30}Zr_{70}$) and Cu-rich compositions ($Cu_{80}Zr_{20}$ – $Cu_{90}Zr_{10}$) and increments of 5 at. % in the middle of the composition space ($Cu_{40}Zr_{60}$ – $Cu_{75}Zr_{25}$) due to the presence of experimental glass-formers in this regime. Stable starting structures for each composition were created by expanding a Cu_5Zr unit cell (Space Group 216) to 34,992 atoms and randomly assigning the atomic identities to match the target composition. All simulations were performed in an NPT ensemble at a constant pressure of 1 bar and the simulated cooling rates were justified by prior research on the simulation of metallic materials [34].

The starting structures were rapidly heated to 2700 K and allowed to equilibrate for 600 ps before being cooled to 2600 K at a constant rate over 3000 ps. The structures were then cooled in 50 K increments down to 350 K. The cooling rate (r_1) and equilibration time (t_e) for each temperature increment are provided in Table 1; slower cooling rates between steps and longer equilibration times at each step were used through the supercooled liquid regime to better facilitate relaxation of the structure. We investigated the structure at three temperatures: 1450 K (liquid), 700 K (undercooled liquid), and 350 K (disordered solid).

Table 1
Equilibration times (t_e) and cooling rates (r_1) used in the cooling process for MD simulations.

T (K)	t_e (ps)	r_1 (10^{11} K/s)
1600	428	3.52
1550	428	3.52
1500	428	3.52
1450	428	3.52
1400	428	3.52
1350	785	2.94
1300	1142	2.39
1250	1499	1.84
1200	1856	1.28
1150	2213	0.726
1100	2570	0.171
1050	2213	0.726
1000	1856	1.28
950	1499	1.84
900	1142	2.39
850	785	2.94
800	428	3.52
750	428	3.52
700	428	3.52
650	428	3.52
600	428	3.52
550	428	3.52
500	428	3.52
450	428	3.52
400	428	3.52
350	428	3.52

2.2. Comparison of representative motifs

The 1450 K, 700 K, and 350 K structures of each composition were analyzed with the PPM/HDBSCAN approach described elsewhere [9,15,16]. This approach uses PPM to geometrically align local structures to one another, resulting in an N x N dissimilarity matrix where N is the number of local structures investigated in a given simulation cell. Then, HDBSCAN is applied to this matrix to extract groups of structures that are geometrically similar to one another. In order for the PPM alignment to be effective, this methodology normalizes the interatomic distances in each local structure by the largest distance between the central atom and a neighboring atom in that cluster. Note that this normalization minimizes the effect of thermal disorder as a function of temperature and allows us to compare motifs from across the temperature domain space to one another.

Using this approach, between 6 and 8 representative atomic cluster "motifs" were identified at each temperature and composition, with each motif describing the nearest neighbor atomic arrangements of between 0.4 % - 35.8 % of the atoms in the simulation cell. To enable comparison of the motifs across simulation cells, artificial x-ray diffraction (XRD) patterns were simulated for each motif using the Visualization for Electronic and Structural Analysis (VESTA) software [35] using Cu-Kα radiation. To construct a periodic structure capable of producing a diffraction pattern, we first determined the principal axes of the smallest ellipsoid encompassing each motif. Each motif was then repeated on a cubic lattice, with the cube edge directions aligned with the ellipsoid axes and the cube edge length defined by the longest principal axis. Artificial diffraction patterns were calculated for each motif assuming that these structural units expand in all three dimensions (Fig. 1), providing a "structural fingerprint" for each motif. Note that the patterns derived above are simply a means to obtain motif fingerprints that can be quantitatively compared; they do not represent the medium- or long-range structure of the material, and therefore are not directly comparable with experimental diffraction patterns.

To determine the similarity between two structural fingerprints (patterns A and B), we compare the intensity and position of individual peaks in each simulated diffraction pattern. To be deemed a "match" we required that the peak intensity of a given reflection be at least 5 % of the

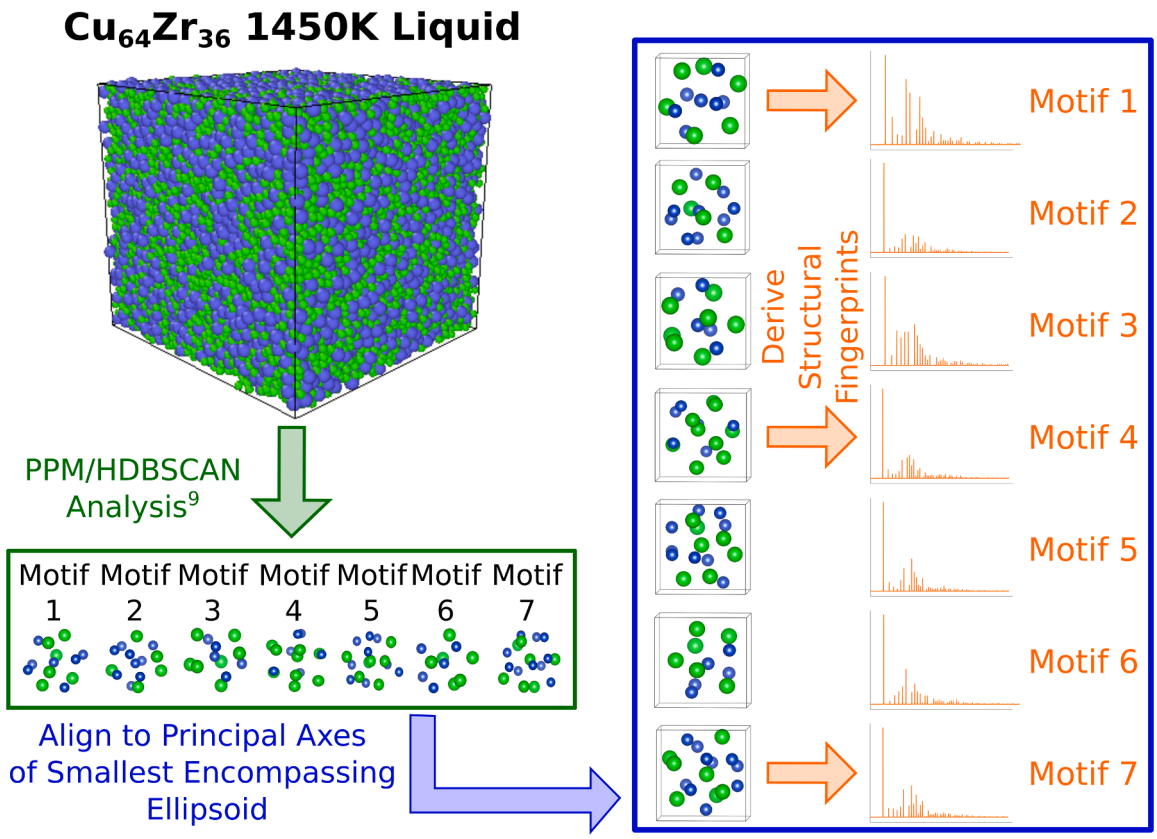

Fig. 1. Illustration of the process for constructing structural fingerprints, using the $Cu_{64}Zr_{36}$ 1450 K liquid as an example. PPM/HDBSCAN motifs are extracted from the simulated structure [9] and the principal axis of their smallest encompassing ellipsoid are identified. The motif is then repeated on a cubic lattice aligned with these principal axes, and a simulated diffraction pattern is calculated for each motif.

maximum intensities in the respective patterns, and that the 2θ peak position agreed to within 0.5°. We then calculate the fraction of matched peaks ($frac_{A,B}$) and the average intensity of the matched peaks ($intensity_{A,B}$):

$$frac_{A,B} = \frac{m_{A,B}}{n_A} \tag{1}$$

$$intensity_{A,B} = \frac{\sum_{j=0}^{m_{A,B}} I_{j,A}}{m_{A,B}} \tag{2}$$

In Eqs. (1) and (2), n_A and $m_{A,B}$ correspond to the total number of peaks in pattern A and the number of matched peaks between patterns A and B, respectively, while $I_{j,A}$ is the intensity of the relevant matched peak in pattern A. To quantitatively describe the correlation between patterns A and B, we then calculate the product of these parameters, C_{AB}, where a higher value corresponds to a higher degree of agreement between the patterns:

$$C_{AB} = frac_{A,B} \times intensity_{A,B} = \frac{\sum_{j=0}^{m_{A,B}} I_{j,A}}{n_A} \tag{3}$$

Eq. (3) provides a means to compare the structural fingerprints of all motifs across composition and temperature space. Notably, this fingerprint methodology was applied because it enabled easy comparison of discrete patterns derived from the large number of irregular motif structures, in contrast to the relative difficulty deriving and/or comparing functions such as the structure factor or periodic distribution function.

2.3. Comparison of motifs to standard structures

The similarity of a given motif to standard structure types was quantified by performing polyhedral template matching (PTM) in OVITO [36]. Motifs that had a root-mean squared distance (RMSD) of less than 0.3 relative to hexagonal close-packed (HCP), face-centered cubic (FCC), body-centered cubic (BCC), simple cubic, or icosahedral geometries were deemed "similar" to the associated structure. Note that a motif can meet this criterion for multiple standard structures and the choice of the RMSD limit for similarity is somewhat arbitrary, although previous work has suggested that the appropriate limit is system-dependent [37].

3. Results

A total of 263 motifs were extracted from the 13 compositions and three temperatures investigated. Using Eq. (3), we calculated a 263 × 263 matrix of C_{AB} values comparing every binary combination of structural fingerprints resulting from these motifs, representing over 1,350,000 nearest neighbor structures from across the system (34,992 atoms, 13 compositions, 3 temperatures). Applying HDBSCAN to identify groups with similar C_{AB} values, we found that 228 motifs representing 90.2 % of all atomic clusters fall into 12 representative "super groups", with 35 motifs (132,965 nearest neighbor structures) being classified as "outliers" by the analysis. That is, although the outlier motifs each represent significant fractions of their respective simulation cells, they were not similar enough to motifs from other simulation cells to be grouped together. Note that this super grouping process applied to all 263 motifs combined 51 motifs that were initially separated within their respective simulation cells. The structural fingerprints are grouped accordingly in Fig. 2, where Groups 1–3 each include 40 or more motifs, Groups 4–6 each include 20–26 motifs, and the remaining super groups each include less than 10 motifs. The fingerprints for the outlier motifs are also shown for completeness.

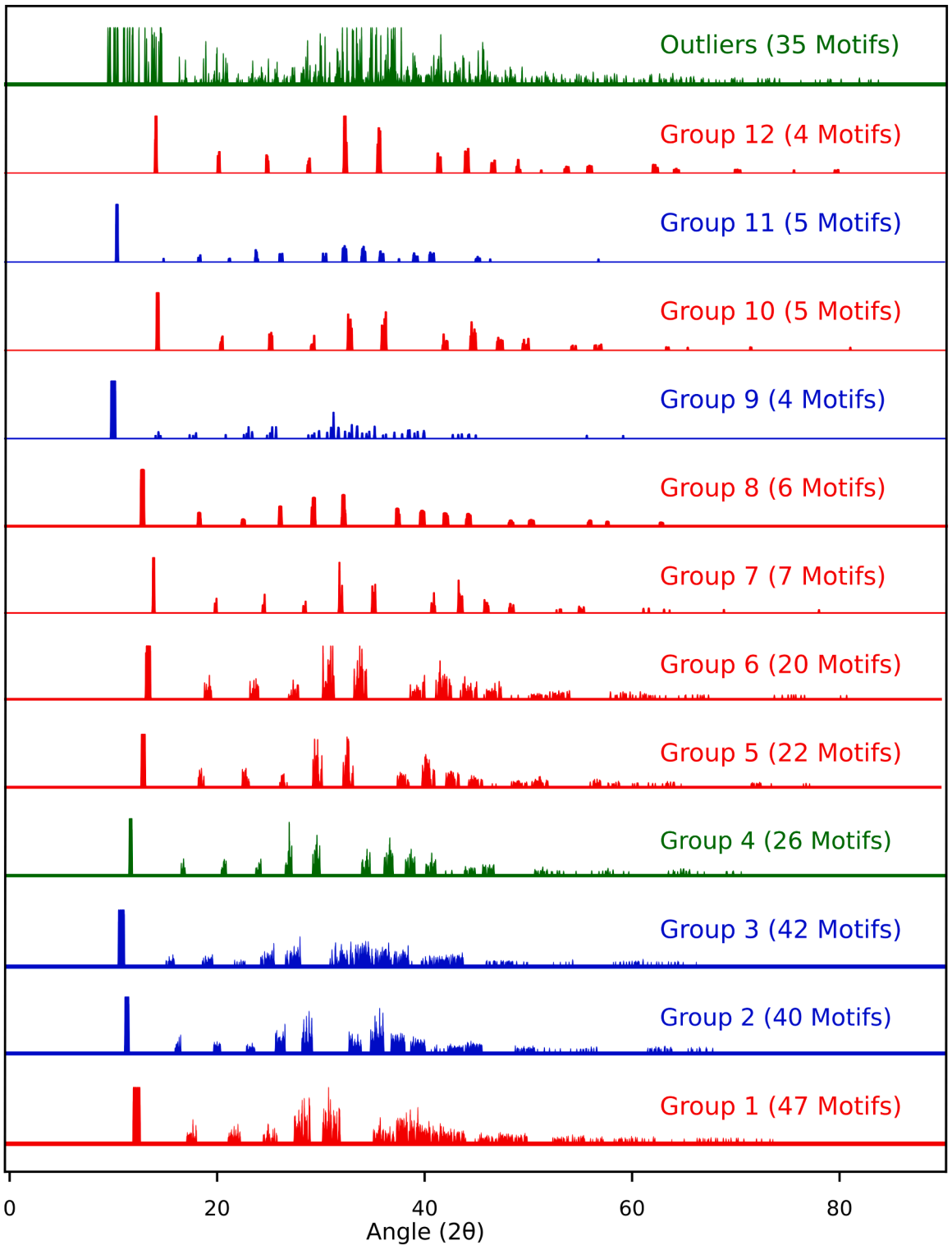

Fig. 2. The structural fingerprints of the 12 PPM/HDBSCAN super groups are shown, representing 263 motifs spanning 13 alloy compositions and 3 temperatures. The number of motifs included in each super group are indicated in parentheses. Groups that are predominantly made up of Cu-centered, Zr-centered, and equiatomic structures are colored red, blue, and green, respectively.

4. Discussion

The results described in Fig. 2 indicate that the short-range atomic structure of Cu-Zr liquids and disordered solids, across all compositions or temperatures, can be described by a surprisingly small number of nearest-neighbor building-blocks. Furthermore, additional work has shown that this behavior is not unique to Cu-Zr alloys [38]. The simulated diffraction patterns of the motifs within each super group exhibit some "peak broadening", since each motif within the super group has similar symmetry but slightly different atomic spacing, depending on the composition of the constituent atomic clusters.

To examine the geometry of the 12 primary building-blocks, we

identified the motif with the highest average C_{AB} value with respect to the rest of the motifs in the super group as an exemplar for that group. We then used the matplotlib library in Python [39] to plot the atomic positions of all atomic clusters associated with a given motif on a 3-dimensional density map. The density maps for the exemplar motifs of each super group are shown in Fig. 3, where color indicates the temperature of the simulation from which each motif was extracted, and the color bar values correlate with the spatial density of data points. The fraction of atoms in the simulation cell associated with each exemplar motif is provided in parentheses. For example, the Group 7 exemplar density map shows over 10,800 clusters (31.1 %) from the simulated $Cu_{90}Zr_{10}$ liquid at 1450 K. In each case, the atoms occupy reasonably well-defined "clouds" around specific positions in the motif, although the atoms rarely occupy the exact same positions relative to the center.

While the density maps provide visual confirmation of the clustering analysis, the number of data points and the deviations in the atomic positions within each cloud make it difficult to draw meaningful conclusions about the symmetry of the exemplar motifs or the differences between them. To make such comparisons easier, we utilized the scikit-learn library in Python to perform a k-means analysis to isolate common atomic positions within these density maps [40] where a silhouette score [41] was used to determine the appropriate number of clusters for the k-means analysis. We then calculated the centroid positions of these k-means groups, the "tightness" of atomic positions around the centroid for a given site, and the "occupation probability" of each site, where the central atomic position is normalized to have an occupation probability of 1.0. This data is shown in Fig. 4, where the size of each data point is directly correlated to the "tightness" of the associated k-means group around the centroid position and the fill color indicates the site occupation probability. An occupation probability of less than one (red) means that some constituent clusters do not have an atom in that spatial area whereas an occupation probability greater than one (blue) indicates that some of the clusters have more than one atom sitting within that cloud group. These can be thought of as describing the likelihood of a "vacancy" or "interstitial" defect at these locations in the motif structures. This centroid-based analysis provides a more quantitative picture of the exemplar structures than the density maps, allowing for the subsequent comparison of the exemplar motifs to one another. The codes used to make both the density and centroid plots are publicly available in the form of a GitHub repository [42].

Examining the site occupation probabilities for each super group, three of the groups (2, 7, and 8) exhibit roughly uniform occupation probability for all sites in the group. Four super groups (4, 5, 10, and 12) exhibit a "clipping" phenomenon, wherein some sites are less than fully occupied. Interestingly, none of the groups that exhibit clipping are predominantly Zr-centered (Fig. 2). This suggests that the smaller radius of a central Cu atom makes it more difficult to accommodate deviations from "ideal" nearest-neighbor positions, resulting in some positions remaining unoccupied. Four more super groups, include two Cu-centered (Groups 1 and 6) and two Zr-centered (Groups 3 and 11) exhibit a "swapping" phenomenon, wherein sites with occupancy less than one are balanced by another site with occupancy greater than one. Finally, the Zr-centered Group 9 exhibits a unique phenomenon wherein several sites on one side of the group have an occupation probability greater than one, indicating an ability to accommodate an extra atom on that side of the cluster. Notably, this is one of the smaller super groups, comprised of only 4 motifs, suggesting that this is an unusual phenomenon. Descriptions of the various types of site occupancies are summarized in Table 2.

Inspired by the Voronoi tessellation method commonly used to describe disordered atomic structures, we constructed a Voronoi polyhedron for the exemplar motif for each super group and described its symmetry using Voronoi indices, where the indices indicate the number of polyhedron faces with 3, 4, 5, and 6 edges or vertices, respectively. Regardless of temperature or composition, all of the super groups, representing 90.2 % of the nearest-neighbor atomic clusters in the investigated systems, are characterized by pure icosahedral (⟨0,0,12,0⟩, Group 2) or quasi-icosahedral geometries: ⟨0,2,8,1⟩ (Groups 4, 5, 10, and 12), ⟨0,1,10,2⟩ (Groups 1, 6, and 11), ⟨1,0,9,3⟩ (Group 3), ⟨0,3,6,3⟩ (Group 7), ⟨0,2,8,2⟩ (Group 8), and ⟨0,1,10,4⟩ (Group 9) [26–31]. PTM further indicates that the exemplars for these super groups meet the criteria for similarity to the icosahedral geometry while failing to meet these criteria for the other standard geometries. Of the local structures represented by the 35 outlier motifs, more than 80 % are similar to HCP, BCC, FCC, and simple cubic geometries, as shown in Fig. 5. Less than 10 % of the outlier structures are similar to the icosahedral geometry, with this number approaching zero at the lowest temperature. The remaining motifs are dissimilar to all considered standards. This analysis suggests that the outlier structures result from the frustrated long-range packing of icosahedra, represented by the super group motifs.

The differences among the super groups are summarized in Table 3. We first note that Groups 2, 3, 7, 8, and 9 each have unique Voronoi indices, indicative of differences in their nearest-neighbor atomic arrangements. The remaining super groups have indices of ⟨0,2,8,1⟩ (Groups 4, 5, 10, and 12) or ⟨0,1,10,2⟩ (Groups 1, 6, and 11). We next focus on deconvoluting these super groups based on central atom type and the observed occupation probabilities of each site in the exemplar motif.

All four ⟨0,2,8,1⟩-type super groups exhibit a clipped structure. In Groups 4, 10, and 12, this clipping is symmetric, with sites on opposite sides of the cluster unoccupied in approximately half of the constituent structures, as indicated by site occupancies of approximately 0.5 in Fig. 4. In contrast, Group 5 exhibits clipping at four asymmetric sites, distinguishing it from the other ⟨0,2,8,1⟩ groups. Group 4 is evenly split between Cu- and Zr-centered clusters, distinguishing it from Groups 10 and 12, which are both predominantly Cu-centered (Fig. 2). The distinguishing features between Groups 10 and 12 are not readily apparent from the current analysis; the simulated diffraction peaks for Group 10 are shifted to slightly higher values of 2θ relative to Group 12 in Fig. 2, suggesting that a small adjustment in the peak-matching requirements may have changed the C_{AB} values sufficiently to result in the combination of these groups.

Unlike the clipped ⟨0,2,8,1⟩ exemplars, all three ⟨0,1,10,2⟩ structures exhibit swapping. Group 1 exhibits a symmetric 1-to-1 swap of an atom from one side to the other. In contrast, Groups 6 and 11 swap from two neighboring sites on one side of the structure, where the occupancy ranges from 0.7 to 0.85, to a site on the opposite side, where the occupancy is close to 1.5. Groups 6 and 11 are further distinguished by the stark contrast in predominant central atom type, with Group 6 being predominantly Cu-centered and Group 11 predominantly Zr-centered as described in Table 3.

Finally, we consider how the population of the 12 common building-blocks and the 35 outlier motifs vary with composition and temperature. This data is summarized in Table S1. Generally, Cu-centered clusters are more common for Cu-rich compositions, and Zr-centered clusters are more common for Zr-rich compositions. Notably, Groups 7–12 are significantly less common than Groups 1–6; although these groups combine 4–7 motifs from multiple systems, they are only observed over very limited composition ranges. While the efficient icosahedral-like packing of these groups explains their presence across multiple systems, their main role seems to be to balance the composition as necessary. In contrast, Groups 1–6, which each combine 20 or more motifs, are each much more prevalent across a wider range of compositions. This suggests that these clusters provide the true backbone of each macroscopically disordered system.

While there are apparent trends in super group population with composition, there are no obvious trends in the population of any group with temperature. This is likely the result of both the relatively small simulation cell size and the fast quenching limiting the degree of structural relaxation as the temperature decreases. However, the outlier motifs become noticeably more common as the temperature decreases. At 1450 K, only 6 of the 13 investigated compositions include outlier

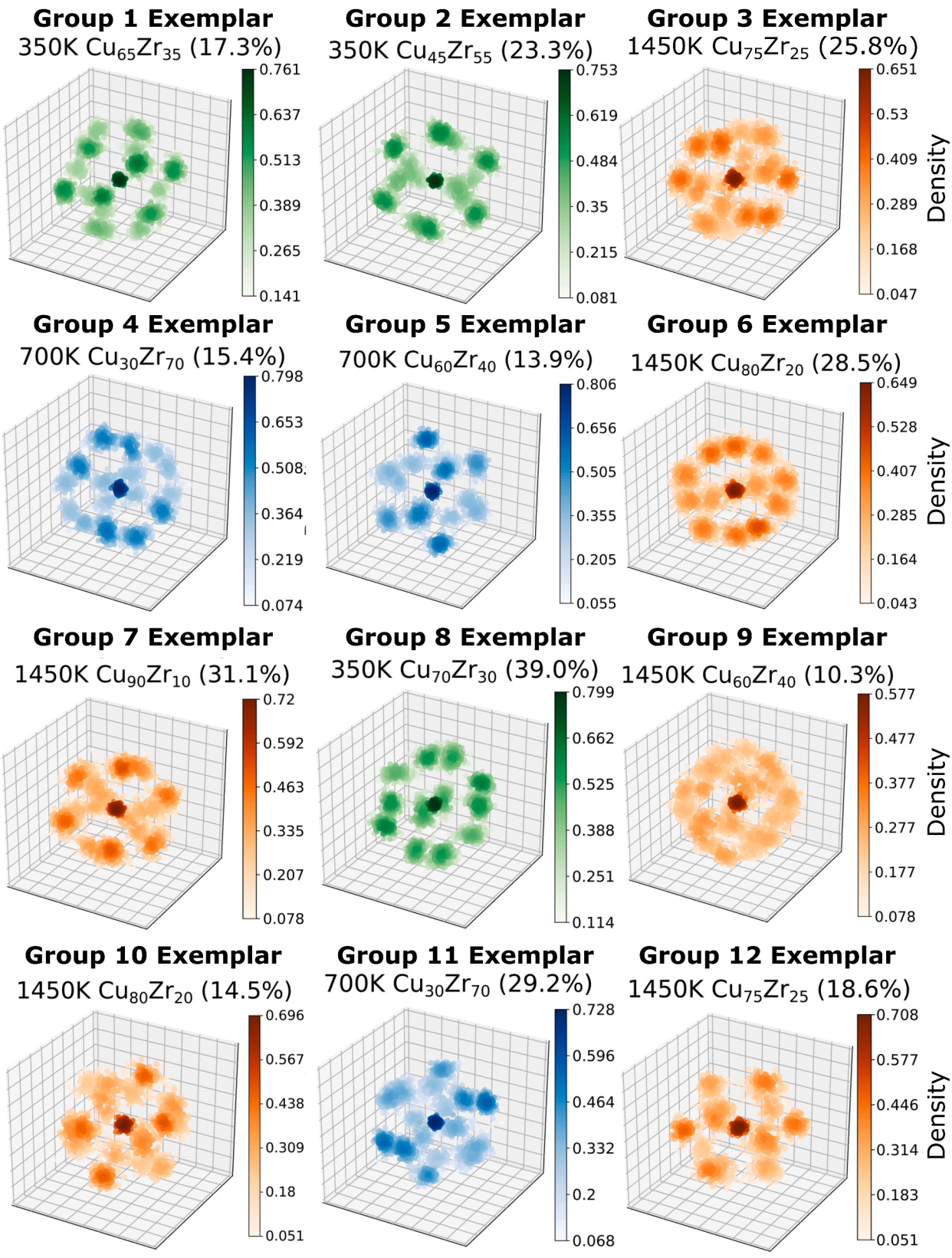

Fig. 3. Density plots for each of the 12 PPM/HDBSCAN super groups, illustrating the positions of all atoms from the simulation cell corresponding to the exemplar motif representing that group. The values in parentheses indicate the fraction of atoms associated with the exemplar motif in the corresponding simulation cell.

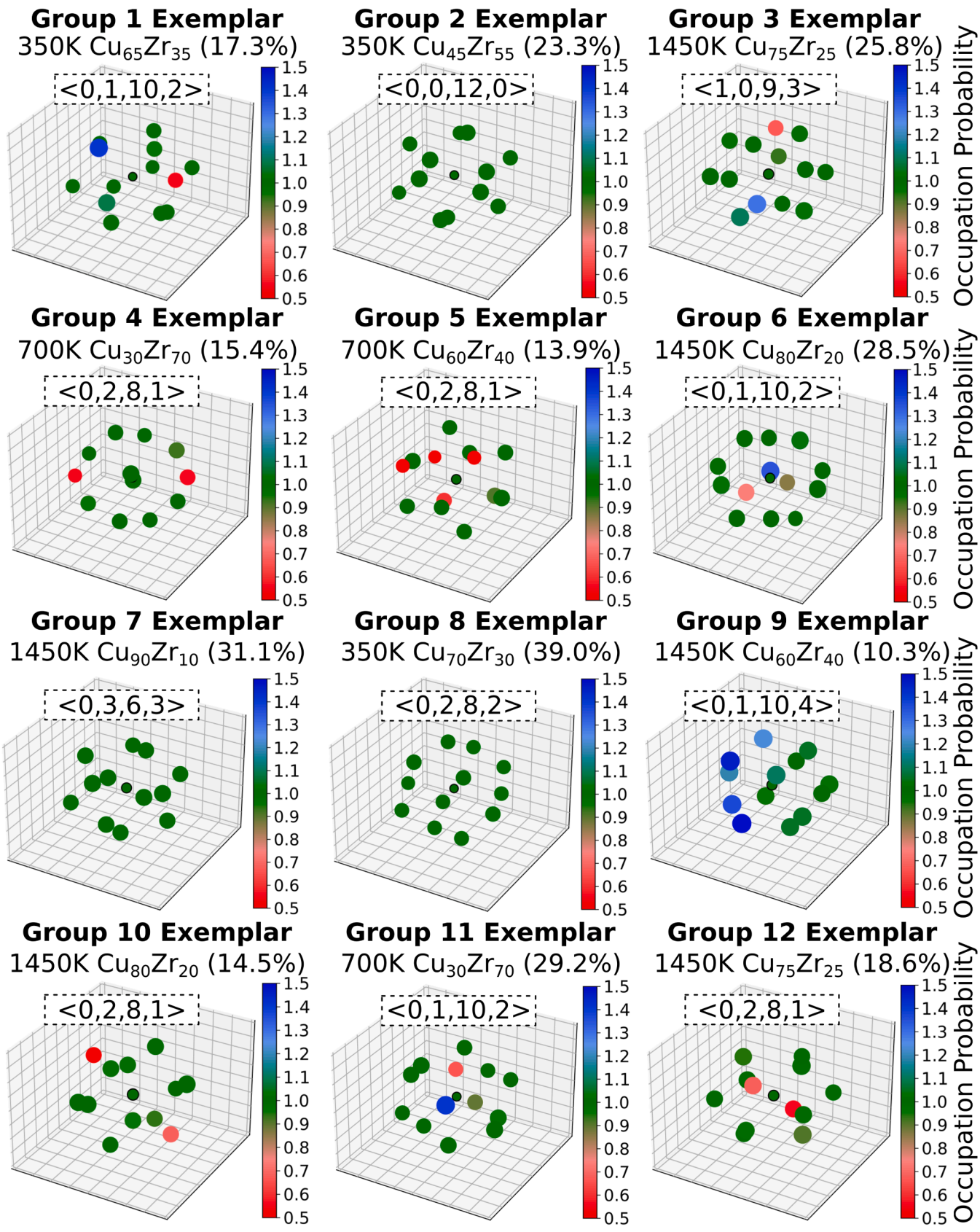

Fig. 4. K-means centroid plots for exemplar motifs from 12 PPM/HDBSCAN super groups, where the size of the data points represents the spatial density of the atoms at each position and the color corresponds to the "occupation probability" of each site. The values in parentheses indicate the fraction of atoms associated with the exemplar motif in the corresponding simulation cell.

Table 2
Description of the atomic cluster site occupancy patterns observed in Fig. 4.

Occupancy pattern	Description	HDBSCAN super groups
"Uniform", U	All sites in the cluster are approximately uniformly occupied in all constituent structures.	2, 7, 8
"Clipping"	*Atoms are "clipped" or missing in some of the constituent clusters.*	
CL1	Symmetric "clipping" of exactly two sites.	4, 10, 12
CL2	Asymmetric "clipping" of multiple sites	5
"Swapping"	*Atoms "swap" from one position to another.*	
SW1	1-to-1 symmetric "swap" across the cluster.	1, 3
SW2	2-to-1 "swap" across the cluster, from 2 sites on one side to 1 site on the other.	6, 11
Other	–	
"Enriched", EN	Enrichment of certain sites without corresponding decrease in occupation probability elsewhere in the cluster (opposite of "clipping")	9

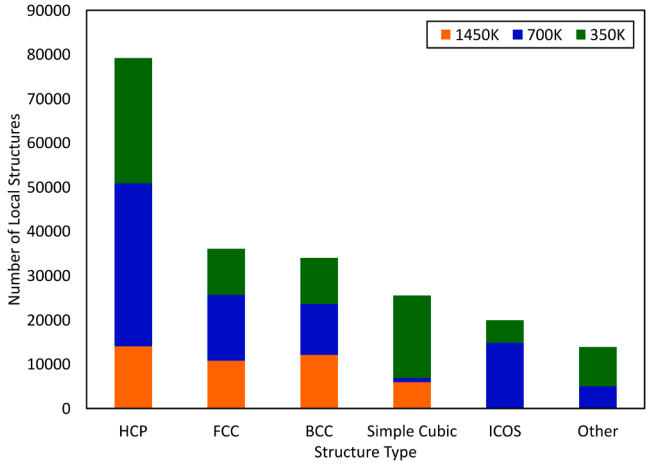

Fig. 5. Number of outlier motifs that exhibit an RMSD < 0.3 relative to standard geometries by polyhedral template matching, as a function of temperature. Those labeled "Other" are structures than failed to meet the RMSD criteria for any of the standard geometries.

motifs; this increases to 9 compositions at 700 K, and 12 compositions at 350 K. This reflects the need for more non-icosahedral clusters to "fill the gaps" between icosahedra to accommodate the lack of translational order as the system moves further away from equilibrium.

The prevalence of icosahedral ordering in Cu-Zr and similar glasses has been noted previously. Simulations by Sheng et al. showed that icosahedral order is expected when the atomic radius ratio of the components is approximately 0.9, consistent with the Cu-Zr system [17]. Such icosahedral order in metallic glasses also has been experimentally observed via nanodiffraction techniques [17–22] with Hirata et al. showing experimental evidence of ⟨0,2,8,0⟩ and ⟨0,2,8,1⟩ geometries in Ni-Zr metallic glasses, a system closely related to Cu-Zr [18]. Various prior work has also examined the evolution of icosahedral-like structures upon cooling [16,19,43–45] with Zhang et al. showing that the level of icosahedral order in a simulated $Cu_{64}Zr_{36}$ glass approaches 27 % as simulated cooling rates approach more realistic levels [45]. Lu et al., on the other hand, suggest that such icosahedral/icosahedral-like order is not the primary driver of GFA in Cu-Zr alloys [46]. As noted above, the present work aligns with Lu et al.'s observation and does not show clear trends in the populations of the various icosahedral or quasi-icosahedral super groups with temperature, although these structures make up a majority of the system at all temperatures. In addition to the small simulation cell size and fast quenching making such trends difficult to discern, the density-based clustering and super grouping processes inherently combine nearest neighbor structures that are similar but not identical in atomic arrangement, in contrast to the prior studies. Thus, this clustering process allows for some thermal distortions or strain in the clusters, potentially masking the previously observed evolution with temperature. Future work will consider the development of such local strains during quenching and their role in glass formation and properties.

Beyond the strong agreement with previous reports of icosahedral order, the present work is unique in that the analysis extends across both temperature and composition space to show a surprising level of continuity among Cu-Zr short-range structures. As noted by Kramer and Li, "the emerging consensus is that undercooled metallic liquids and glasses show a profound sensitivity to composition" such that the structural continuity observed here is surprising [44]. Both the concept of the "outlier" motifs that differ from the fundamental building blocks and the observations of variations in the site occupancies within the super groups are not reported in prior literature and may provide a clear basis for describing "defects" in the disordered structure. For instance, variations in site occupancies suggest a method to quantify the population and distribution of point defects (akin to vacancies and interstitial atoms), which control many of the properties of crystalline materials, ranging from their creep response to electronic and optical behavior. While the concept of point defects has been applied to covalent glasses [47], to our knowledge this is the first observation of a similar feature in the more densely packed metallic glasses. Outlier motifs, analogous to the geometrically unfavored motifs identified by Ma [48], are somewhat higher-order defects and may form the basis for flow defects such as shear transformation zones [49–55]. Ongoing work will investigate the distribution of such defects and their role in the behavior of disordered metallic materials.

5. Conclusions

In this work, we have shown that a high fraction (90.2 %) of nearest-

Table 3
Summary of Voronoi polyhedron indices, central atom type, and site occupancy pattern descriptor for the exemplar motif from each HDBSCAN super group.

HDBSCAN super group	Number of motifs	Number of clusters	Voronoi indices	Cu-centered (%)	Zr-centered (%)	Occupancy pattern
Group 1	47	245,948	<0,1,10,2>	73.4	26.6	SW1
Group 2	40	241,003	<0,0,12,0>	27.9	72.1	U
Group 3	42	197,482	<1,0,9,3>	19.4	80.6	SW1
Group 4	26	132,545	<0,2,8,1>	50.0	50.0	CL1
Group 5	22	129,547	<0,2,8,1>	78.8	21.2	CL2
Group 6	20	117,095	<0,1,10,2>	89.0	11.0	SW2
Group 7	7	36,309	<0,3,6,3>	92.5	7.50	U
Group 8	6	32,437	<0,2,8,2>	85.4	14.6	U
Group 9	4	26,957	<0,1,10,4>	18.5	81.5	EN
Group 10	5	24,770	<0,2,8,1>	91.5	8.50	CL1
Group 11	5	23,383	<0,1,10,2>	3.80	96.2	SW2
Group 12	4	13,938	<0,2,8,1>	93.4	6.60	CL1
Outliers	35	131,796	–	43.6	56.4	–

neighbor atomic clusters in disordered Cu-Zr liquids and solids can be effectively described by 12 common nearest-neighbor atomic arrangements, regardless of temperature or composition. All but two arrangements are distinguished by their combinations of Voronoi polyhedron geometry, central atom type, and site occupation pattern. All 12 "building-blocks" exhibit icosahedral or quasi-icosahedral geometries, suggesting a very high fraction of icosahedral-like structures in all disordered Cu-Zr alloys, regardless of the glass forming ability of the composition, suggesting that icosahedral order is not the primary driver of GFA in Cu-Zr alloys. In contrast, the remaining 9.8 % of the atomic clusters are predominantly represented by HCP-like, FCC-like, or BCC-like structures that are not common across temperatures and compositions. While the most common building-blocks likely form the backbone of disordered Cu-Zr structures, these outlier motifs are important for accommodating the lack of long-range translational order in the predominantly icosahedral packing.

Although three of the common building-blocks, including the perfect ⟨0,0,12,0⟩ icosahedron, had uniform occupancy of all sites in the structure, most groups exhibited symmetrically arranged sites with occupancies greater or less than one. These observations explain why Voronoi tessellation alone is insufficient to describe the geometry of nearest-neighbor structures; clearly, structures that are identified as geometrically similar by the PPM/HDBSCAN approach often exhibit differences in coordination number or atomic positions that would lead to significant variation in the Voronoi indices of the constituent structures despite their structural similarity.

Declaration of Competing Interest

The authors declare that they have no known competing financial interests or personal relationships that could have appeared to influence the work reported in this paper.

Acknowledgements

This work was supported by the National Science Foundation under Grant No. DMR-2004630. MD simulations and subsequent analyses were performed using the Washington University Center for High Performance Computing, which is partially supported through NIH grant S10OD018091.

Supplementary materials

Supplementary material associated with this article can be found, in the online version, at doi:10.1016/j.actamat.2023.119624.

References

[1] C.A. Schuh, T.C. Hufnagel, U. Ramamurty, Mechanical behavior of amorphous alloys, Acta Mater. 55 (2007) 4067–4109, https://doi.org/10.1016/j.actamat.2007.01.052.
[2] J. Schroers, Processing of bulk metallic glass, Adv. Mater. 22 (2010) 1566–1597, https://doi.org/10.1002/adma.200902776.
[3] J.D. Bernal, J. Mason, Packing of spheres: co-ordination of randomly packed spheres, Nature 188 (1960) 910–911, https://doi.org/10.1038/188910a0.
[4] J.D. Bernal, Geometry of the structure of monatomic liquids, Nature 185 (1960) 68–70.
[5] J.L. Finney, Random packings and the structure of simple liquids. I. The geometry of random close packing, Proc. R. Soc. London. A. Math. Phys. Sci. 319 (1970) 479–493, https://doi.org/10.1098/rspa.1970.0189.
[6] C.H. Bennett, Serially deposited amorphous aggregates of hard spheres, J. Appl. Phys. 43 (1972) 2727–2734, https://doi.org/10.1063/1.1661585.
[7] P.H. Gaskell, A new structural model for amorphous transition metal silicides, borides, phosphides and carbides, J. Non. Cryst. Solids 32 (1979) 207–224, https://doi.org/10.1016/0022-3093(79)90073-5.
[8] A.K. Varshneya, Fundamentals of Inorganic Glasses, 2nd ed., Academic Press, 1994 https://doi.org/10.1016/C2009-0-21359-6.
[9] W.P. Weeks, K.M. Flores, Using characteristic structural motifs in metallic liquids to predict glass forming ability, Intermetallics 145 (2022), 107560, https://doi.org/10.1016/J.INTERMET.2022.107560.
[10] Y. Li, Q. Guo, J.A. Kalb, C.V. Thompson, Matching glass-forming ability with the density of the amorphous phase, Science 322 (1979) (2008) 1816–1819, https://doi.org/10.1126/science.1163062.
[11] G. Duan, D. Xu, Q. Zhang, G. Zhang, T. Cagin, W.L. Johnson, W.A. Goddard, Molecular dynamics study of the binary Cu46Zr54 metallic glass motivated by experiments: glass formation and atomic-level structure, Phys. Rev. B Condens. Matter. Mater. Phys. 71 (2005), 224208, https://doi.org/10.1103/PhysRevB.71.224208.
[12] O.J. Kwon, Y.C. Kim, K.B. Kim, Y.K. Lee, E. Fleury, Formation of amorphous phase in the binary Cu-Zr alloy system, Metal Mater. Int. 12 (2006) 207–212, https://doi.org/10.1007/BF03027532.
[13] P. Tsai, K.M. Flores, A laser deposition strategy for the efficient identification of glass-forming alloys, Metall Mater. Trans. A Phys. Metall Mater. Sci. 46 (2015) 3876–3882, https://doi.org/10.1007/s11661-015-2900-x.
[14] P. Tsai, K.M. Flores, A combinatorial strategy for metallic glass design via laser deposition, Intermetallics 55 (2014) 162–166, https://doi.org/10.1016/j.intermet.2014.07.017.
[15] A.D. Banadaki, J.J. Maldonis, P.M. Voyles, S. Patala, Point-Pattern Matching Technique For Local Structural Analysis in Condensed Matter, 2018. http://arxiv.org/abs/1811.06098 (accessed October 21, 2019).
[16] J.J. Maldonis, A.D. Banadaki, S. Patala, P.M. Voyles, Short-range order structure motifs learned from an atomistic model of a Zr50Cu45Al5 metallic glass, Acta Mater. 175 (2019) 35–45, https://doi.org/10.1016/j.actamat.2019.05.002.
[17] H.W. Sheng, W.K. Luo, F.M. Alamgir, J.M. Bai, E. Ma, Atomic packing and short-to-medium-range order in metallic glasses, Nature 439 (2006) 419–425, https://doi.org/10.1038/nature04421.
[18] A. Hirata, P. Guan, T. Fujita, Y. Hirotsu, A. Inoue, A.R. Yavari, T. Sakurai, M. Chen, Direct observation of local atomic order in a metallic glass, Nat. Mater. 10 (2011) 28–33, https://doi.org/10.1038/nmat2897.
[19] J. Saida, M. Matsushita, T. Zhang, A. Inoue, M.W. Chen, T. Sakurai, Precipitation of icosahedral phase from a supercooled liquid region in Zr65Cu7.5Al7.5Ni10Ag10 metallic glass, Appl. Phys. Lett. 75 (1999) 3497–3499, https://doi.org/10.1063/1.125367.
[20] A. Hirata, L.J. Kang, T. Fujita, B. Klumov, K. Matsue, M. Kotani, A.R. Yavari, M. W. Chen, Geometric frustration of icosahedron in metallic glasses, Science (1979) 341 (2013) 376–379, https://doi.org/10.1126/science.1232450.
[21] S.O. Hruszkewycz, T. Fujita, M.W. Chen, T.C. Hufnagel, Selected area nanodiffraction fluctuation electron microscopy for studying structural order in amorphous solids, Scr. Mater. 58 (2008) 303–306, https://doi.org/10.1016/j.scriptamat.2007.10.009.
[22] A. Hirata, Local structure analysis of amorphous materials by angstrom-beam electron diffraction, Microscopy 70 (2021) 171–177, https://doi.org/10.1093/jmicro/dfaa075.
[23] V. Wessels, A.K. Gangopadhyay, K.K. Sahu, R.W. Hyers, S.M. Canepari, J.R. Rogers, M.J. Kramer, A.I. Goldman, D. Robinson, J.W. Lee, J.R. Morris, K.F. Kelton, Rapid chemical and topological ordering in supercooled liquid Cu 46Zr54, Phys. Rev. B Condens. Matter Mater. Phys. 83 (2011), 094116, https://doi.org/10.1103/PhysRevB.83.094116.
[24] R. Dai, J.C. Neuefeind, D.G. Quirinale, K.F. Kelton, X-ray and neutron scattering measurements of ordering in a Cu 46 Zr 54 liquid, J. Chem. Phys. 152 (2020), 164503, https://doi.org/10.1063/5.0003816.
[25] Y.Q. Cheng, E. Ma, H.W. Sheng, Alloying strongly influences the structure, dynamics, and glass forming ability of metallic supercooled liquids, Appl. Phys. Lett. 93 (2008), 111913, https://doi.org/10.1063/1.2987727.
[26] H.L. Peng, M.Z. Li, W.H. Wang, C.-Z. Wang, K.M. Ho, Effect of local structures and atomic packing on glass forming ability in CuxZr100−x metallic glasses, Appl. Phys. Lett. 96 (2010), 021901, https://doi.org/10.1063/1.3282800.
[27] K.V. Reddy, S. Pal, Evaluation of glass forming ability of Zr–Nb alloy systems through liquid fragility and Voronoi cluster analysis, Comput. Mater. Sci. 158 (2019) 324–332, https://doi.org/10.1016/j.commatsci.2018.11.045.
[28] X. Hui, H.Z. Fang, G.L. Chen, S.L. Shang, Y. Wang, J.Y. Qin, Z.K. Liu, Atomic structure of Zr41.2Ti13.8Cu12.5Ni10Be22.5 bulk metallic glass alloy, Acta. Mater. 57 (2009) 376–391, https://doi.org/10.1016/j.actamat.2008.09.022.
[29] T. Fujita, K. Konno, W. Zhang, V. Kumar, M. Matsuura, A. Inoue, T. Sakurai, M. W. Chen, Atomic-scale heterogeneity of a multicomponent bulk metallic glass with excellent glass forming ability, Phys. Rev. Lett. 103 (2009), 075502, https://doi.org/10.1103/PhysRevLett.103.075502.
[30] M. Durandurdu, Ab initio modeling of metallic Pd80Si20 glass, Comput. Mater. Sci. 65 (2012) 44–47, https://doi.org/10.1016/j.commatsci.2012.06.040.
[31] F. Li, X.J. Liu, Z.P. Lu, Atomic structural evolution during glass formation of a Cu–Zr binary metallic glass, Comput. Mater. Sci. 85 (2014) 147–153, https://doi.org/10.1016/j.commatsci.2013.12.058.
[32] S. Plimpton, Fast parallel algorithms for short-range molecular dynamics, J. Comput. Phys. 117 (1995) 1–19, https://doi.org/10.1006/JCPH.1995.1039.
[33] M.I. Mendelev, Y. Sun, F. Zhang, C.Z. Wang, K.M. Ho, Development of a semi-empirical potential suitable for molecular dynamics simulation of vitrification in Cu-Zr alloys, J. Chem. Phys. 151 (2019), 214502, https://doi.org/10.1063/1.5131500.
[34] L. Ward, D. Miracle, W. Windl, O.N. Senkov, K. Flores, Structural evolution and kinetics in Cu-Zr metallic liquids from molecular dynamics simulations, Phys. Rev. B. Condens. Matter. Mater. Phys. 88 (2013), 134205, https://doi.org/10.1103/PhysRevB.88.134205.
[35] K. Momma, F. Izumi, VESTA3 For Three-Dimensional Visualization of crystal, Volumet. Morphol. Data 44 (2011) 1272–1276, https://doi.org/10.1107/S0021889811038970. Urn:Issn:0021-8898.

[36] A. Stukowski, Visualization and analysis of atomistic simulation data with OVITO-the open visualization tool, Model. Simul. Mater. Sci. Eng. 18 (2010).
[37] P.M. Larsen, S. Schmidt, J. Schiøtz, Robust structural identification via polyhedral template matching, Model. Simul. Mat. Sci. Eng. 24 (2016), 055007, https://doi.org/10.1088/0965-0393/24/5/055007.
[38] P. Weeks, Structural understanding of glass-forming metallic alloys. McKelvey School of Engineering, Washington University in St. Louis, 2023.
[39] J.D. Hunter, Matplotlib: a 2D graphics environment, Comput. Sci. Eng. 9 (2007) 90–95, https://doi.org/10.1109/MCSE.2007.55.
[40] F. Pedregosa, G. Varoquaux, A. Gramfort, V. Michel, B. Thirion, Scikit-learn: machine learning in Python, J. Mach. Learn. Res. 12 (2011) 2825–2830.
[41] Scikit-learn, Selecting the Number of Clusters With Silhouette Analysis On KMeans Clustering, (n.d.). https://scikit-learn.org/stable/auto_examples/cluster/plot_kmeans_silhouette_analysis.html.
[42] W.P. Weeks, 3D_Plots Github Repository, (n.d.). https://github.com/weekswp/3D_Cloud_Plots.
[43] X.W. Fang, C.Z. Wang, S.G. Hao, M.J. Kramer, Y.X. Yao, M.I. Mendelev, Z.J. Ding, R.E. Napolitano, K.M. Ho, Spatially resolved distribution function and the medium-range order in metallic liquid and glass, Sci. Rep. 1 (2011) 1–5, https://doi.org/10.1038/srep00194.
[44] M.J. Kramer, M. Li, Changes in short- and medium-range order in metallic liquids during undercooling, MRS Bull. 45 (2020) 943–950, https://doi.org/10.1557/mrs.2020.272.
[45] Y. Zhang, F. Zhang, C.Z. Wang, M.I. Mendelev, M.J. Kramer, K.M. Ho, Cooling rates dependence of medium-range order development in Cu64.5Zr35.5 metallic glass, Phys. Rev. B. Condens. Matter. Mater. Phys. 91 (2015), 064105, https://doi.org/10.1103/PhysRevB.91.064105.
[46] B.F. Lu, L.T. Kong, K.J. Laws, W.Q. Xu, Z. Jiang, Y.Y. Huang, M. Ferry, J.F. Li, Y. H. Zhou, EXAFS and molecular dynamics simulation studies of Cu-Zr metallic glass: short-to-medium range order and glass forming ability, Mater. Charact. 141 (2018) 41–48, https://doi.org/10.1016/j.matchar.2018.04.036.
[47] S.A. Dembovsky, E.A. Chechetkina, Defects and glass formation, J. Non. Cryst. Solids. 64 (1984) 95–111, https://doi.org/10.1016/0022-3093(84)90209-6.
[48] E. Ma, Tuning order in disorder, Nat. Mater. 14 (2015) 547–552, https://doi.org/10.1038/nmat4300.
[49] F. Spaepen, A microscopic mechanism for steady state inhomogeneous flow in metallic glasses, Acta Metall. 25 (1977) 407–415, https://doi.org/10.1016/0001-6160(77)90232-2.
[50] A.S. Argon, Plastic deformation in metallic glasses, Acta Metall. 27 (1979) 47–58, https://doi.org/10.1016/0001-6160(79)90055-5.
[51] A.S. Argon, H.Y. Kuo, Plastic flow in a disordered bubble raft (an analog of a metallic glass, Mater. Sci. Eng. 39 (1979) 101–109, https://doi.org/10.1016/0025-5416(79)90174-5.
[52] A.S. Argon, L.T. Shi, Development of visco-plastic deformation in metallic glasses, Acta Metall. 31 (1983) 499–507, https://doi.org/10.1016/0001-6160(83)90038-X.
[53] D. Pan, A. Inoue, T. Sakurai, M.W. Chen, Experimental characterization of shear transformation zones for plastic flow of bulk metallic glasses, Proc. Natl. Acad. Sci. 105 (2008) 14769–14772, https://doi.org/10.1073/pnas.0806051105.
[54] H.B. Yu, W.H. Wang, H.Y. Bai, Y. Wu, M.W. Chen, Relating activation of shear transformation zones to β-relaxations in metallic glasses, Phys. Rev. B. 81 (2010), 220201, https://doi.org/10.1103/PhysRevB.81.220201.
[55] J.D. Ju, D. Jang, A. Nwankpa, M. Atzmon, An atomically quantized hierarchy of shear transformation zones in a metallic glass, J. Appl. Phys. 109 (2011), https://doi.org/10.1063/1.3552300.